forbidden transitions observed in HgXY have approximately half the intensity shown for corresponding transitions in HgX_2, as expected for a reduction in the populations of the ground state by half. The allowed transitions are relatively unaffected. HgXY is, however, expected to be solvated in methanol. Since it is linear, the methanol molecules must be in the equatorial plane about mercury and could be four in number, making an approximately octahedral solvate similar to that suggested for $HgCl_2$ in methanol.[12] But a trigonal-bipyramidal species cannot be ruled out, since the resolved charge-transfer spectrum of $HgCl_3^-$ in water has been assigned to this structure[33] and $[HgCl_3(MeOH)]^-$ has been reported.[12] The readiness with which Cl^- added on could imply the presence of $HgCl_2$ (and HgXY) solvates with one rather than two methanol molecules to be eliminated.

Acknowledgment. We thank the Science Research Council for the purchase of the Cary 14 H spectrophotometer. The digitizing attachment was purchased out of Harwell Contract EMR 1913. We thank the University of Leeds Computing Service for assistance, and R.A.A. acknowledges a Leeds University postgraduate award. T.R.G. thanks the Royal Society for a travel grant and the Chemistry Department, Michigan State University, East Lansing, MI 48824, for hospitality and facilities during the preparation of this paper.

Registry No. HgI_2, 7774-29-0; HgIBr, 13444-76-3; $HgBr_2$, 7789-47-1; HgICl, 13444-77-4; $HgCl_2$, 7487-94-7; HgBrCl, 13595-89-6.

References and Notes

(1) Y. Marcus and I. Eliezer, *Coord. Chem. Rev.*, **4**, 273 (1969).
(2) Y. Marcus, *Acta Chem. Scand.*, **11**, 329, 599, 610, 811 (1957).
(3) T. G. Spiro and D. N. Hume, *J. Am. Chem. Soc.*, **83**, 4305 (1961).
(4) M. L. Delwaulle and F. Francois, *C. R. Hebd. Seances Acad. Sci.*, **208**, 999, 1002 (1939).
(5) R. E. Dessy and Y. K. Lee, *J. Am. Chem. Soc.*, **82**, 689 (1960).
(6) M. Zangen and Y. Marcus, *Isr. J. Chem.*, **2**, 91 (1964).
(7) M. L. Delwaulle, *Proc. Colloq. Spectrosc. Int., 6th*, 565 (1956).
(8) M. L. Delwaulle, *Bull. Soc. Chim. Fr.*, 1294 (1955), and references therein.
(9) L. Newman and D. N. Hume, *J. Am. Chem. Soc.*, **79**, 4571 (1957).
(10) J. A. Rolfe, D. E. Sheppard, and L. A. Woodward, *Trans. Faraday Soc.*, **50**, 1275 (1954).
(11) G. Allen and E. Warhurst, *Trans. Faraday Soc.*, **54**, 1786 (1958).
(12) Z. Kecki, *Rocz. Chem.*, **36**, 345 (1962).
(13) I. Eliezer, *J. Chem. Phys.*, **42**, 3625 (1965).
(14) O. W. Kolling, *Inorg. Chem.*, **1**, 561 (1962).
(15) G. J. Janz, C. Baddiel, and T. R. Kozlowski, *J. Chem. Phys.*, **40**, 2055 (1964).
(16) M. Zangen, *J. Phys. Chem.*, **69**, 1835 (1965).
(17) T. R. Griffiths and R. A. Anderson, *J. Chem. Soc., Faraday Trans. 2*, **75**, 957 (1979).
(18) T. R. Griffiths and P. J. Potts, *Anal. Chim. Acta*, **71**, 1 (1974).
(19) T. R. Griffiths and P. J. Potts, *Inorg. Chem.*, **14**, 1039 (1975).
(20) T. R. Griffiths and P. J. Potts, *J. Chem. Soc., Dalton Trans.*, 344 (1975).
(21) J. R. Dickinson, T. R. Griffiths, and P. J. Potts, *J. Inorg. Nucl. Chem.*, **37**, 511 (1975).
(22) T. R. Griffiths and P. J. Potts, *J. Inorg. Nucl. Chem.*, **37**, 521 (1975).
(23) A. Savitsky and M. J. Goley, *Anal. Chem.*, **36**, 1627 (1964).
(24) J. Steinier, Y. Termonia, and J. Deltour, *Anal. Chem.*, **44**, 1906 (1972).
(25) J. R. Morrey, *Anal. Chem.*, **40**, 905 (1968).
(26) W. L. Butler and D. W. Hopkins, *Photochem. Photobiol.*, **12**, 439 (1970).
(27) T. R. Griffiths and D. C. Pugh, submitted for publication in *J. Chem. Soc., Faraday Trans. 1*.
(28) R. Fletcher and M. J. D. Powell, *Comput. J.*, **6**, 163 (1963).
(29) W. R. Busing and H. A. Levy, *Commun. ACM*, **6**, 445 (1970).
(30) C. L. Van Panthaleon Van Eck, Thesis, Leiden, 1958.
(31) S. Feldberg, P. Klotz, and L. Newman, *Inorg. Chem.*, **11**, 2860 (1972).
(32) A. D. Walsh, *J. Chem. Soc.*, 2266 (1953), and subsequent papers.
(33) T. R. Griffiths and R. A. Anderson, *J. Chem. Soc., Chem. Commun.*, 61 (1979).

Contribution from the Chemistry Department and Energy and Mineral Resources Research Institute of Iowa State University, Ames, Iowa 50011

Polarized Electronic Absorption Spectra for Dimolybdenum(II) Tetraacetate

DON S. MARTIN,* ROBERT A. NEWMAN, and PHILLIP E. FANWICK

Received November 27, 1978

Polarized spectra with rich vibrational detail are reported for two faces of single crystals of $Mo_2(O_2CCH_3)_4$ at temperatures down to 5 K. Evidence, which includes the orientation in space of transition moments for individual vibrational lines, hot bands, and Franck–Condon factors, is presented that the 23 000-cm^{-1} band is the electric-dipole-allowed $^1A_{2u} \leftarrow {}^1A_{1g}$ or $\delta^* \leftarrow \delta$ with an origin at 21 700 cm^{-1}. However, the intensities are sufficiently low that lines excited vibronically, although somewhat weaker, approach the intensity of the dipole-allowed progression. A second transition at 26 500 cm^{-1} is evident as well from the low-temperature spectra. The spectra of a number of dimeric carboxylate complexes of molybdenum(II) are compared and the possible cause of the exceptionally low intensity for an electric-dipole-allowed transition is discussed.

Introduction

Single-crystal electronic absorption spectra are now available for several compounds which contain dimeric complexes with multiple metal–metal bonds. Studies[1-3] of crystals with $Re_2Cl_8^{2-}$ together with results[4] for $Mo_2Cl_8^{4-}$, which have quadruple metal–metal bonds, have confirmed that the electronic absorption band at the lowest observed energy is polarized with the electric vector of the light wave in the direction of the metal–metal bond. In the D_{4h} symmetry of these ions, the spin-allowed $\delta^* \leftarrow \delta$ excitation is $b_{1u}^* \leftarrow b_{2g}$, and the transition is therefore $^1A_{2u} \leftarrow {}^1A_{1g}$. This transition should be electric dipole allowed for polarization in the direction of the z axis which is coincident with the metal–metal bond. The assignment of the first electronic band to this $\delta^* \leftarrow \delta$ transition is predicted by Xα–scattered wave calculations,[2,5] although the calculated energies for the transition have been generally much lower than the observed values. Polarized crystal spectra[6] for $K_4Mo_2(SO_4)_4 \cdot 2H_2O$, in which the $Mo_2(SO_4)_4^{4-}$ ion has four bridging sulfato ligands, have indicated a band at 19 400 cm^{-1} with a polarization again consistent with a $\delta^* \leftarrow \delta$ assignment. Also, for $K_3Mo_2(SO_4)_4 \cdot 3.5H_2O$, in which one electron from the quadruple bond has been lost by oxidation, the first band with an origin at about 6300 cm^{-1} has the polarization predicted for the $\delta^* \leftarrow \delta$ assignment.[7] The spectra of the chloro and sulfato complexes have, therefore, presented a coherent pattern with the first electronic transition assignments of $\delta^* \leftarrow \delta$.

A group of tetra-μ-carboxylato-dimolybdenum(II) complexes have, however, presented a conflicting situation. These complexes are also generally considered under the D_{4h} point group about the metal–metal bond since the atomic positions out through the α carbon follow this symmetry. The spectra

0020-1669/79/1318-2511$01.00/0

for several of these carboxylato complexes have possessed vibrational structure with much greater resolvable detail than any of the other dimers, except for possibly $K_3Mo_2(SO_4)_4 \cdot 3.5H_2O$; and it has been possible to observe crystal polarizations for a number of individual vibrational lines. In spectra, recorded in our laboratory for tetra-μ-glycine-dimolybdate(II) sulfate tetrahydrate[8] and for tetra-μ-formato-dimolybdenum(II),[6] the lowest energy electronic band was not comprised of vibrational progressions whose polarizations would be only along the metal–metal bond. It was concluded therefore that the first band was likely not $\delta^* \leftarrow \delta$, $^1A_{2u} \leftarrow {}^1A_{1g}$.

Meanwhile Trogler et al.[9] have reported polarized crystal spectra for tetra-μ-acetato-dimolybdenum(II) and unpolarized powder spectra of tetrakis[μ-(trifluoroacetato)]-dimolybdenum(II). In their report they proposed that the first electronic band is $\pi^* \leftarrow \delta$, $^1E_g \leftarrow {}^1A_{1g}$. A part of the complexity of the very rich vibrational structure in their spectra was attributed to the splitting of the ^1E_g excited state by the local ligand or crystal field. The dimeric complexes in these two compounds occupy $\bar{1}$ sites in triclinic crystals. However, Trogler et al. did not suitably reconcile some features of the crystal optics which are exceptionally critical for consideration of these triclinic crystals.

The present paper presents an extensive study of crystal optical features and absorption spectra for $Mo_2(O_2CCH_3)_4$. The results have indicated that the first electronic transition may well be the $\delta^* \leftarrow \delta$, $^1A_{2u} \leftarrow {}^1A_{1g}$ which, although electronic dipole allowed, has such a low transition moment that vibronic (Herzberg–Teller) excitation has a comparable intensity.

Experimental Section

Exceptionally fine crystals for spectroscopy were obtained by the following method. $Mo(CO_6)$ was dissolved in *o*-dichlorobenzene. An excess of glacial acetic acid with some acetic anhydride was added to this solution. The mixture was refluxed for 20 h at ca. 176 °C with a stream of dry nitrogen bubbling through the solution to exclude oxygen. Following the refluxing, the mixture in the flask was cooled very slowly overnight without removal of the heating mantle as a crop of bright yellow crystals formed. The crystals were filtered onto a glass frit and washed with absolute ethanol and with ether. Crystals would deteriorate in air in a few weeks but large crystals have been stored in a vacuum desiccator for more than 1 year with retention of good optical properties. The crystals were mostly needles. They invariably exhibited two easily distinguishable faces, as Trogler et al.[9] described. In one face, the extinction between crossed polarizers was close (within 0–2°) to the needle axis whereas for the other face the extinction was 11–13° from the needle axis. It was observed under white light, however, that the extinctions were not sharp for either face. Thus, as the crystal was rotated through the extinction, the color would pass from a red to blue or vice versa, indicative of a fairly strong wavelength dependence for the extinction direction. This effect was more pronounced for the face with the 11–13° extinction. Such behavior is recognized as possible for a general face of any biaxial crystal.

Several crystals were cemented to fibers for mounting on a computer-controlled X-ray diffractometer. From a series of rotation photographs, standard programs were utilized to establish a set of triclinic axes. The cell parameters were refined from a set of reflections and were invariably in good agreement with the values reported for a triclinic cell by Cotton et al., viz., $a:b:c$ = 8.418 Å:5.500 Å:7.529 Å and $\alpha:\beta:\gamma$ = 84.13°:105.24°:106.00°. The long needle axis was found to be the b axis, again in agreement with Trogler et al. Various reflections could be called into diffracting orientations for the identification of the faces. It was observed that the faces with extinctions close to the needle (b) axis were invariably 001 or 00$\bar{1}$ faces whereas the others with extinctions 11–13° off the b axis were 100 or $\bar{1}$00. This disagrees with the face assignments of Trogler et al. so we have checked these assignments for several crystals on the diffractometer.

Upon inspection of the preparations, several crystalline needles have been discovered which had very thin sections projecting from one end of the needle. Whereas the needles might be 100–200 μm thick, the thin sections were less than 5 μm thick. The optical extinctions and absorptions of the thin sections were exactly aligned with those of the needle, so the evidence indicated that these needles and thin sections were each part of a single crystal. With some of these crystals, after spectra were recorded, the crystals were mounted for face identification on the X-ray diffractometer.

The thickness of large crystals was measured by a calibrated scale in the eyepiece of a microscope.

The thickness of thin crystals was determined by the phase difference in transmitted light waves indicated by a Leitz–Wetzlar tilting crystal compensator in a polarizing microscope. These measurements were performed at a wavelength of 546.1 nm provided by an interference filter. The birefringence was obtained from the indices of refraction determined by the Becke line method with a set of Cargille Co. refractive index standards for the 546.1-nm line. These indices were as follows: 100 face, 1.672 and 1.634; 001 face, 1.671 and 1.631. In each face the high index was for the extinction direction closer to the b axis.

The equipment for recording polarized spectra at various temperatures has been described previously.[7,11] Because the optical extinctions might be a function of wavelength, spectra were recorded with a series of settings of the polarizer, which was placed in the light beam from the monochromator that was incident on the face of the crystal.

Spectra with highly resolved vibrational features were recorded with slit settings that provided a dispersion of no more than 0.12 nm. The lowest available scan speed of 0.05 nm/s was utilized. Absorbances were punched each 0.1 nm on cards for computer processing and plotting. This procedure, used to prepare the figures presented, does give a reasonably good representation of important features, but some details were more clearly evident and accurately presented on the recorder charts.

Results and Discussion

Consideration of Crystal Optics. Single-crystal absorption spectra are usually treated on the basis of the well-known phenomenon that in the absence of optical activity for nonabsorbing crystals, light of any wavelength is transmitted through the crystal as two independent plane waves polarized in orthogonal planes. The two planes of polarization are indicated by the "extinction" directions between crossed polarizers. If the two waves are absorbed differently, the maximum and minimum in the absorption will occur with the polarizers aligned with these extinction directions. It is usually convenient, if possible, to set the polarizer angle where maximum absorption of a strongly dichroic band is observed, and at 90° to this angle, for recording spectra. This check was considered especially important for $Mo_2(O_2CCH_3)_4$, since the microscopic observations indicated an observable wavelength dependence of the extinction direction. When the intensity of individual vibration lines in the low-temperature spectra were measured as a function of polarizer angle, it was found that the line intensities maximized a considerable angle away from an extinction observed under the polarizing microscope.

Spectra of the low-energy region of the band were therefore recorded for a temperature of 5 K at a series of polarizer angles with increments no larger than 10° through 180°. Several of these spectra are shown for the 001 face and the 100 face in Figures 1 and 2, respectively. A number of vibrational progressions are evident from the spectra, and important lines have been labeled. Wavenumbers of resolvable vibrational peaks and shoulders have been recorded in Table I. The lowest energy feature in the spectra is a line at 21 700 cm^{-1} (A_0 in Table I which is the origin of a progression for which five additional terms are also listed). Other strong progressions, labeled C and E, have origins 275 and 545 cm^{-1}, respectively, above A_0. In addition, there are a number of weaker progressions, only some of which are labeled in Figures 1 and 2.

Polarizer angles in the figures have been shown as the angle in degrees measured in a clockwise direction, as observed from

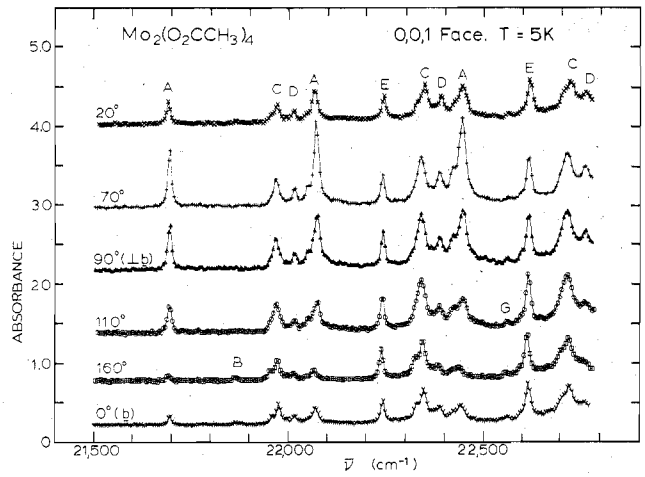

Figure 1. Absorption spectra at various polarization angles for the 001 face of $Mo_2(O_2CCH_3)_4$. The crystal was 4.2 μm thick, and absorbances can be converted to molar absorptivities by multiplying the absorbance by 463 M^{-1} cm^{-1}: 70 and 160° closest spectra to A_{max} and A_{min}; 110 and 20° closest spectra to E_{max} and E_{min}, respectively.

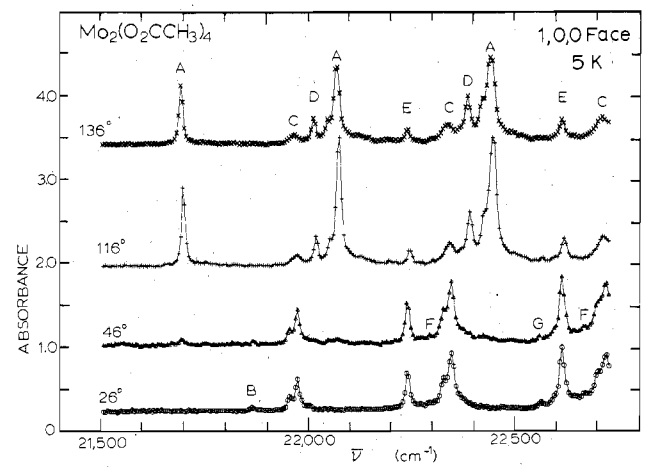

Figure 2. Absorption spectra at various polarization angles for the 100 face of $Mo_2(O_2CCH_3)_4$. The crystal was 3.8 μm thick, and absorbances can be converted to molar absorptivities by multiplying by 490 M^{-1} cm^{-1}: 116 and 26° are closest spectra to A_{max} and A_{min} while 46 and 136° are closest to E_{max} and E_{min}, respectively.

the direction of the entering light beam on the 100 or the 001 faces. For the $\bar{1}00$ or $00\bar{1}$ faces rotation would be in the opposite directions. Trogler et al. apparently recorded spectra for the 001 face. The 0° (b) and 90° ($\perp b$) spectra in Figure 1 appear to agree very well with their spectra, although some additional features can be recognized in the present plots. It is evident in Figure 1 that the A peak at 70° is clearly higher than that at 90°, and accordingly the A peak is smaller at 160° than at 0°. On the other hand, although not clearly evident, the E peak was higher at 110° than at 70 or 90° and lower at 20° than at 0 or 160°. Thus, it was observed that the A peaks and the E peaks attained maxima and minima at well-separated polarization angles for both the 001 and the 100 faces, and the polarizations for these maxima and minima were significantly removed from the optical extinctions seen at room temperature between crossed polarizers.

The preceding observations suggested that perhaps the assumption of plane polarization for the traversing light waves should be questioned. It is recognized from classical electromagnetic theory[12] that for an absorbing monoclinic or triclinic crystal, the principal axes of the indicatrix for the imaginary part of the refractive index (absorption) do not necessarily coincide with the axes of the indicatrix of the real part. In such case, an incident plane polarized light wave will

Table I. Vibrational Details in the Absorption Spectra of $Mo_2(O_2CCH_3)_4$

progression	$\bar{\nu}$, cm^{-1}	$\Delta\bar{\nu}$,[a] cm^{-1}
A-1	21 300	−400
C'	21 405	(−295)
C-1	21 575	−400
A_0	21 700	
	21 725 sh	(25)
	21 760 vw	(60)
	21 780 vw	(80)
	21 830 vw	(130)
B_0	21 875 w	(175)
	21 955 w	(255)
C_0	21 975	(275)
D_0	22 020	(320)
	22 055	(355)
A_1	22 075	375
E_0	22 245	(545)
F_0	22 290 vw	(590)
	22 325 w	370
C_1	22 345	370
D_1	22 390	370
	22 425	370
A_2	22 445	370
G_0	22 565	(865)
	22 600 sh	(900)
E_1	22 620	375
F_1	22 665 vw	375
	22 700 w	375
C_2	22 720	375
D_2	22 765	375
A_3	22 820	375
G_1	22 935 w	370
E_2	22 985	360
C_3	23 085	365
D_3	23 135	370
A_4	23 185	365
G_2	23 310 w	375
E_3	23 360	375
C_4	23 455	370
D_4	22 495	360
A_5	23 550	365
G_3	23 680 w	370
E_4	23 735	375

[a] Values in parentheses give the difference $\Delta\bar{\nu}$ from the A_0 line. Values without parentheses give the difference $\Delta\nu$ from the preceding line in the progression.

be transmitted as two elliptically polarized waves. The major and minor axes for the two waves are mutually perpendicular, and their orientation is influenced by both the real and imaginary parts of the refractive indices. The A peaks are some of the most intense absorption features in the $Mo_2(O_2CCH_3)_4$ spectra. It can be seen from Figure 2 that the A intensity virtually disappears at 26°; therefore it can be concluded that ellipticity of the light at the wavelength of this band must be sufficiently great that it can be considered essentially a plane wave. The rotation of the vibration planes evident from the spectra must therefore result from variations in the real part of the refractive indices, which are recognized to fluctuate in the vicinity of absorption regions.

The A_0 and E_0 peaks were well separated from other strong absorption lines. Hence the height of these peaks above the level of recorded absorbance in their proximity has been plotted in Figure 3 for the two faces. A procedure utilized by Stewart and Davidson[13] served to evaluate the intensity of absorption and the orientation of the plane waves at each of these peaks. The absorbance, Ab, is related to polarization angle, φ, by the expression

$$10^{-Ab} = 10^{-Ab_{max}} \cos^2(\varphi - \theta) + 10^{-Ab_{min}} \sin^2(\varphi - \theta) \qquad (1)$$

where Ab_{max} and Ab_{min} are the absorption intensities of the two plane waves and θ is the polarization angle for the wave with the higher absorption, Ab_{max}. Values for Ab_{max}, Ab_{min},

Table II. Least-Squares Values of Absorption Parameters for the A and E Origin Peaks of $Mo_2(O_2CCH_3)_4$

	$A_0(100)$	$E_0(100)$	$A_0(001)$	$E_0(001)$
Ab_{max}/L, μm^{-1}	0.284 ± 0.008	0.142 ± 0.007	0.196 ± 0.004	0.109 ± 0.005
Ab_{min}/L, μm^{-1}	0.003 ± 0.004	0.041 ± 0.005	0.021 ± 0.002	0.071 ± 0.005
θ, deg	115 ± 1	134 ± 3	68 ± 1	113 ± 5
Ab_{max}/Ab_{min}	83.1	3.38	9.36	1.51

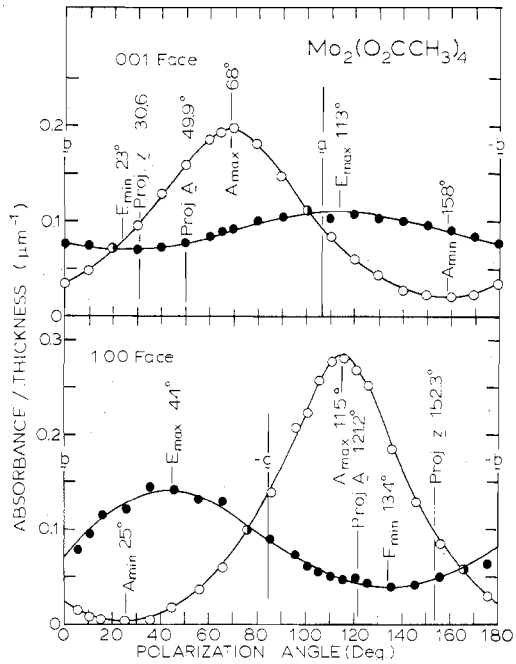

Figure 3. Peak heights recorded for the A_0 and E_0 peaks for the 001 and 100 faces as a function of polarizer angle. Open circles are for the A_0 peak and solid circles are for the E_0 peak. Curves are least-squares fit.

and θ were then determined by a nonlinear least-squares treatment of the data. In Table II are presented values for Ab_{max}/L, Ab_{min}/L and θ (where L is the crystal thickness) from the least-squares computation for the A_0 and E_0 peaks of each face. For the A_0 peaks, which have very high polarization ratios, the orientation of the vibration planes was determined with an uncertainty of only ±1°. The planes for the E peak with much lower polarization ratios are given with the much larger uncertainty of ±3–5°.

Orientation of Transition Moments. A transition moment may be assigned to the absorption of radiation from the v^0th vibration level of a ground state (g) to the v'th vibrational level of an excited state (f). Within the Born–Oppenheimer approximation this transition moment is given by the expression

$$\mathbf{M}_{gv^0,fv'} = \langle \chi_{v^0}(...Q_i...)\psi_g(...x_j...Q_i...)|\sum e\mathbf{r}|\psi_f(...x_j...Q_i...)\chi_{v'}(...Q_i...)\rangle \quad (2)$$

where the $...x_j...$ are electron coordinates, $...Q_i...$ are normal vibrational coordinates of the nuclei, and $\sum e\mathbf{r}$ is the usual dipole operator, a function of the electron coordinates. $\mathbf{M}_{gv^0,fv'}$ is a vector quantity, and the intensity of the absorption is proportional to the square of the length of this vector. The intensity of absorption of a plane wave should be proportional to the square of the cosine of the angle between $\mathbf{M}_{gv^0,fv'}$ and the electric vector of the wave. For the absorption in a face the expression used is

$$\frac{Ab_{max}}{Ab_{min}} = \frac{\cos^2\theta_1}{\cos^2\theta_2} = \frac{\cos^2\theta'_1}{\cos^2\theta'_2} \quad (3)$$

where θ_1 and θ_2 are the angles between $\mathbf{M}_{fv^0,gv'}$ and the direction of the maximum and minimum polarizations, respectively. θ'_1 and θ'_2 are the angles between the projection of $\mathbf{M}_{gv^0,fv'}$ in the crystal face and the directions of the maximum and minimum polarizations.

If the absorptions are observed for only one face, the orientation of $\mathbf{M}_{gv^0,fv'}$ cannot be determined. Rather, the molecular transition moment is assigned to the various molecular symmetry axes. Then, the polarization ratio is calculated to determine which gives the best agreement with the observed ratio, Ab_{max}/Ab_{min}.

Molecular $Mo_2(O_2CCH_3)_4$ possesses D_{4h} point group symmetry. Therefore a line will appear in the molecular spectrum when the product of the total electronic–vibrational wave functions in eq 2, viz., $\chi_{v^0}\psi_g\psi_f\chi_{v'}$, is a basis function for A_{2u} or E_u. For the case of the A_{2u} product, the transition moment will be aligned along the molecular z axis, i.e., the metal–metal bond. For the E_u product, there will be two transitions of equal energy, with two transition moments of equal magnitude which are orthogonal to each other and orthogonal to the z axis. However, the two moments can in principle have any orientation in the plane perpendicular to z, provided their equality and orthogonality properties are maintained. For such a case, it can be shown that

$$\left(\frac{Ab_{max}}{Ab_{min}}\right)_{x,y} = \frac{\sin^2\theta_1}{\sin^2\theta_2} \quad (4)$$

where θ_1 and θ_2 are the angles between the molecular z axis and the direction of the maximum and minimum polarizations for the face. The molecule of $Mo_2(O_2CCH_3)_4$ occupies a site of much lower symmetry than D_{4h}, viz., $\bar{1}$ in the crystal. The crystal fields therefore may compromise the molecular symmetry. Many more transition moments may now be nonzero. Transition moments may also be shifted in space. The degenerate transitions under D_{4h} may now be separated in energy, and the orthogonality of the two transition moments is no longer required. In such cases crystal spectra will retain their value to the extent that the crystal field perturbations to the D_{4h} symmetry are sufficiently small. The shifts in transition energies and moments will then not be so great but that impositions of molecular symmetry can still be recognized, even though they are not absolute.

The availability of intensities for two faces of crystals has provided considerably more information about the transition moment orientation than the spectra of a single face. For the A_0 peak the polarization ratios, Ab_{max}/Ab_{min}, were 9.36 and 83.1 for the 001 and 100 faces, respectively. Since the dihedral angle between these faces is 75.8°, such high polarization ratios in these two faces would not be possible for a degenerate pair of equal orthonormal transition moments. Hence, the A_0 peak is considered due to a single transition moment. From eq 3, since $[\theta'_2] = |90° - \theta'_1]$, the transition moment is required to be in a plane normal to the 001 face which cuts the 001 face at the angle $\cot^{-1}(9.36^{1/2})$ or 18.1° away from the $A_{max}(001)$ direction. There are, of course, two possible such planes, one on each side of $A_{max}(001)$. From the polarization ratio of 83.1 for the 100 face, the transition moment must lie in either of two planes normal to this face which cut it at angles of 6.3° away from $A_{max}(100)$. The intersection of the two planes normal to 001 with the two normal to 100 give four possible orientations for the A_0 transition moment. A choice between these four possible

orientations can be now based on the relative intensities in the two faces. This ratio should be given by the square of the ratio of the vector dot products

$$A_{max}(100)L(001)/A_{max}(001)L(100) = [\hat{\mathbf{A}}\cdot\hat{\mathbf{A}}_{max}(100)/\hat{\mathbf{A}}\cdot\hat{\mathbf{A}}_{max}(001)]^2 \quad (5)$$

where $\hat{\mathbf{A}}$ is a unit vector in the direction of the transition moment, $\hat{\mathbf{A}}_{max}$ and $\hat{\mathbf{A}}_{min}$ are unit vectors in the indicated polarization directions, and the L's are the crystal thicknesses. Calculated values for the four possible ratios are 1.69, 0.19, 0.049, and 4.40. The observed value, evident from Figure 3, was 1.42. Accordingly, the first vector gives by far the best agreement with the observed ratio and has been taken as $\hat{\mathbf{A}}$, the unit vector which defines the direction of the A_0 transition moment. The projections of this vector for both faces are shown in Figure 3, which also includes the projection of the molecular axis, **z**, on each face. $\hat{\mathbf{A}}$ is oriented in space some 33.9° away from **z**. We have concluded therefore that the A progression represents a series of single transition vibrational lines with z polarizations, for which the molecular polarization has been shifted from the molecular axis by the crystal field perturbations. If these correspond to one member of a degenerate pair, split by the crystal field, as Trogler et al.[9] proposed, it would correspond to a shift from the molecular polarization which must be 90° to z.

The data from the E peak were treated similarly, on the basis of the assumption that it was due to a single nondegenerate transition. Again, the intersection of four planes yielded four possible transition moment vectors, which gave ratios between the two faces of 1.39, 14.1, 0.108, and 1.10. Since the experimental ratio was 1.31, the second and third vectors could be eliminated, but either first and fourth seemed feasible, although the first gave somewhat better agreement with experiment. The first vector proved to be 88.5° away from the molecular axis and 87.0° away from $\hat{\mathbf{A}}$, whereas the fourth vector was 66.3° away from the molecular axis and 47.7° away from $\hat{\mathbf{A}}$.

The C and the D peaks have other absorption features near them, so a quantitative least-squares treatment of their absorbance vs. polarization angle was not attempted. However, it can be seen qualitatively from Figures 1 and 2, and it was still more evident from the total set of spectra that the D peaks followed the polarization of the A peaks and the C peaks followed closely the polarization of the E peaks. Hence, if C and E each represent a single transition, normal to the z molecular axis, which has been split away from another member of a degenerate pair, there appear to be no other lines in the crystal spectra of comparable intensity corresponding to the other transition. Moreover, although a pair of normal transition moments for a truly degenerate transition might give a high polarization ratio for either of the 100 or 001 faces, it would then be required to yield a low polarization ratio for the other face. The low value of 1.52 for the 001 face suggests that E might therefore be due to such a pair of degenerate molecular transitions. For consideration of this possibility, a unit vector $\hat{\mathbf{N}}$ was defined which would be perpendicular to a pair of equal and normal transition moments. For true molecular x,y polarized transitions, $\hat{N}$ would be the z molecular axis. The polarization ratio for each face in accordance with eq 4 was given by the expression

$$\frac{E_{max}}{E_{min}} = \frac{\sin^2\theta_1}{\sin^2\theta_2} = \left(\frac{\hat{\mathbf{N}}\times\hat{\mathbf{E}}_{max}}{\hat{\mathbf{N}}\times\hat{\mathbf{E}}_{min}}\right)^2 \quad (6)$$

where $\hat{\mathbf{E}}_{max}$ and $\hat{\mathbf{E}}_{min}$ are unit vectors in the polarization directions. The substitution of the polarization ratios for the E_0 peak in the 100 and the 001 faces into expression 5 gave two equations involving the three components of the $\hat{\mathbf{N}}$ vector and the normalization requirement of $\hat{\mathbf{N}}$ provided a third equation. The three equations were solved by reiterative numerical methods to give two unique vectors $\hat{\mathbf{N}}_1$ and $\hat{\mathbf{N}}_2$ which satisfied the three equations. The vectors, $-\hat{\mathbf{N}}_1$ and $-\hat{\mathbf{N}}_2$, were also satisfactory but did not represent different transition moments. Values of $E_{max}(100)/E_{max}(001)$ were calculated to be 1.26 and 0.99 for $\hat{\mathbf{N}}_1$, and $\hat{\mathbf{N}}_2$, respectively, so although $\hat{\mathbf{N}}_1$ appeared better, $\hat{\mathbf{N}}_2$ was not really eliminated. $\hat{\mathbf{N}}_1$ was oriented at 32.3° away from the molecular z axis and 64.2° away from **A**. $\hat{\mathbf{N}}_2$ on the other hand was 26.5° away from the molecular z axis and only 10.6° away from $\hat{\mathbf{A}}$.

It appears that the preceding observations are consistent with the proposal that the E_0 peak corresponds to a pair of degenerate transitions with molecular x,y polarization which have not been split in energy by the crystal field. However, the direction and perhaps magnitude of the transition moments have been altered, although both transition moments are approximately normal to each other and are of approximately the same magnitude. A vector normal to each of the transition moments probably lies close to $\hat{\mathbf{N}}_2$ and approximately 10° away from $\hat{\mathbf{A}}$. The C peaks are also attributed to a degenerate pair of molecular x,y polarized transitions.

There is another transition at 21 955 cm^{-1}, only 20 cm^{-1} below the C_0 peak. However, this transition is weaker in both faces than C_0 and therefore is considered another transition, rather than a transition which as been split out from a degenerate pair. Although its intensity vs. polarization follows the C line in the 100 face, it is quite different in the 001 face.

Hot Bands. The preceding analysis has indicated electronic excitation to discrete vibrational states with either molecular z or x,y polarization. It is therefore possible that this band is an electric-dipole-forbidden transition excited by vibronic (Herzberg–Teller) perturbations. On the other hand, the first observed absorption feature at the temperature of 5 K, A_0 at 21 700 cm^{-1}, is the origin of clearly the most intense progression; although it is not an order of magnitude more intense than the C or E progressions. There is the possibility this electronic band is a dipole-allowed $^1A_{2u} \leftarrow {}^1A_{1g}$ transition which possesses such a small static electric dipole transition moment that it only yields intensities comparable to some vibronically excited lines. To distinguish between these two options, we undertook a study of the hot bands. These hot bands are comprised of absorptions which can be measured as the temperature is raised at longer wavelengths than the lowest energy low-temperature feature. Thick crystals are required for observation of these bands, since in order to obtain resolvable peaks, only minor population of the excited vibrational states can be allowed. The lines that might be resolved in hot bands are shown in the energy level diagram of Figure 4. If this is an allowed transition, $^1A_{2u} \leftarrow {}^1A_{1g}$, then the lowest observed absorption at helium temperatures, A_0, is the 0–0 transition. The A progression arises as successive vibrational states $\bar{\nu}_1'$, $2\bar{\nu}_1'$, $3\bar{\nu}_1'$, etc. are excited where $\bar{\nu}_1'$ is the wavenumber for a totally symmetric vibration (A_{1g}) in the excited electronic state. The strong progressions each have a separation of lines amounting to 370 ± 5 cm^{-1}. This vibration in the dimeric complexes has generally been assigned to the metal–metal stretching vibration. Raman measurements,[14] for $Mo_2(O_2CCH_3)_4$ have placed the metal–metal stretch in the ground state at 406 cm^{-1}. The lower value for the excited state is consistent with the expected relaxation of the bonds. The high intensity of successive terms in the progressions based on this vibration, only one of several A_{1g} vibrations, requires a large positional deviation of the atoms in the excited electronic states from their positions in the ground state.

As the temperature of a crystal is raised, a line, broadened somewhat by thermal factors, should appear at an energy $\bar{\nu}_1{}^0$ or 406 cm^{-1} below A_0. The molecular polarization of this line

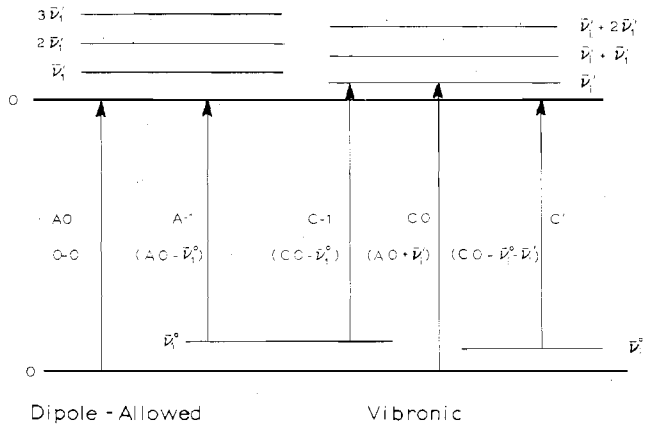

Figure 4. Vibrational lines expected in hot bands for an electric dipole-allowed and a vibronically excited electronic transition with $\bar{\nu}_1$ the wavenumber for an A_{1g} vibration with a high Franck–Condon factor and with $\bar{\nu}_i$ the wavenumber for an exciting vibration in a dipole-forbidden vibronic (Herzberg–Teller) transition.

should be the same as A_0. The intensity of the line is proportional to the population of the first excited vibrational state and also to a Franck–Condon factor. Hence, totally symmetric vibrations with small Franck–Condon factors will not be expected to give observable hot bands. No other hot band of comparable intensity will be expected with the A molecular polarization in the spectra with a dipole-allowed transition.

For a vibronically allowed transition the origin of the progression, shown as C_0 in Figure 4, is at an energy of $\bar{\nu}_i$ above the 0–0 energy, and its progression corresponds to successive excitation of the $\bar{\nu}_1'$ vibration. For this line two hot bands should be developed as the crystal temperature is raised. One band will originate from the $\bar{\nu}_1{}^0$ energy, as shown in Figure 4, and should be at an energy $\bar{\nu}_1{}^0$ or 406 cm^{-1} below C_0. The second band will have an energy $\bar{\nu}_i{}^0 + \bar{\nu}_i'$ below C_0 or $\bar{\nu}_i{}^0$ below the 0–0 line. Both hot bands should have the same molecular polarization as the C_0 line.

Hot bands were recorded at various temperatures from 85 to 175 K, as well as at 5 K for the 001 and the 100 faces at various polarizations. The greatest differences were noted between spectra recorded near the $A_{0_{max}}$ and the $A_{0_{min}}$ polarizations and these spectra are shown in Figure 5 and Figure 6 for the 001 and the 100 faces, respectively. The spectra for the 100 face are probably more informative because the A_0 peak has such low intensity in the 25° polarization. Hence, there is little interference from it. At the polarization of 115° for the 100 face there are two peaks evident. Both undergo a small blue shift as the temperature is decreased and both are discernible in the 85 K spectrum. The lower energy peak at 85 K is at 21 300 cm^{-1} and the other peak at 21 405 cm^{-1}. At 25° polarization the 21 300-cm^{-1} peak is absent but the 21 405-cm^{-1} peak is more intense than at 115°. In addition, a band with a maximum at higher energy can be clearly seen at 125 and 150 K. It could also be observed on the recorder chart at 100 K at 21 575 cm^{-1} although it is not definitely discernible in the computer plot of Figure 6. The 21 300-cm^{-1} and 21 405-cm^{-1} peaks are clearly evident in the 68° polarization of the 001 face in Figure 5 for the somewhat thicker crystal. The 21 300-cm^{-1} peak has much lower intensity at 158° but is still discernible at 100 K. Since the A_0 peak retains greater intensity for A_{min}, the rise in absorption masks the 21 575-cm^{-1} band somewhat; but careful inspection does reveal its presence at 125 K, and perhaps somewhat more clearly in the 100 K spectrum. The bands at 21 300 and 21 405 cm^{-1} agree closely with the hot bands seen by Trogler et al.,[9] but they did not resolve the 21 575-cm^{-1} band.

The single hot band which follows the A polarization is just 400 cm^{-1} below A_0, well within the experimental uncertainty

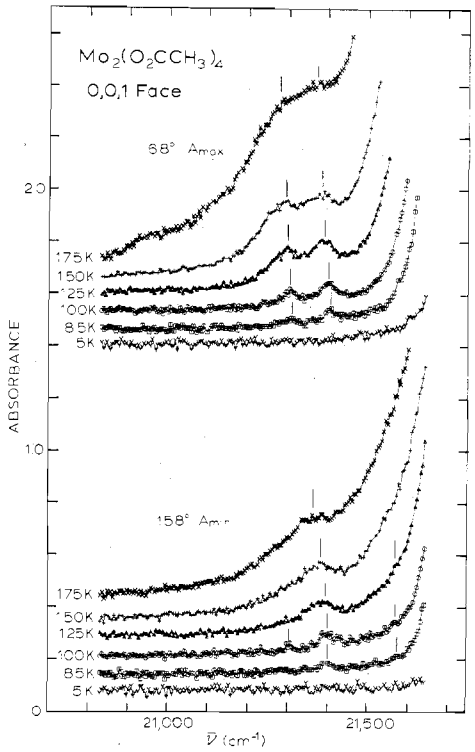

Figure 5. Hot bands recorded for the 001 face of a $Mo_2(O_2CCH_3)_4$ crystal that was 220 μm thick.

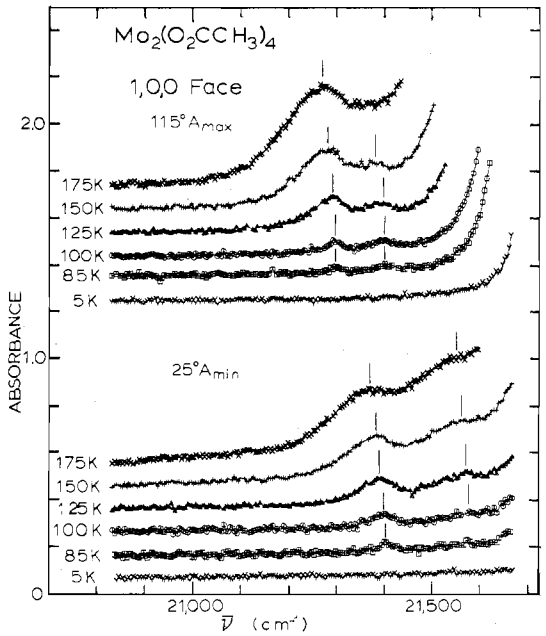

Figure 6. Hot bands recorded for the 100 face of a $Mo_2(O_2CCH_3)_4$ crystal that was 164 μm thick.

for $\bar{\nu}_1{}^0$. On the other hand, two peaks are observed which follow the C–E polarization. The C_0 peak is the first major feature above A_0 and the hot bands from the C transitions are therefore expected to be the only ones observable at sufficiently low temperatures for adequate resolution to be retained. The 21 575-cm^{-1} peak is just 400 cm^{-1} below C_0 and has been labeled C-1. The 21 405-cm^{-1} peak is 295 cm^{-1} below A_0 and has been labeled C'. This pattern is exactly that shown in Figure 4 and provides strong evidence that this band is likely an electric-dipole-allowed transition, $^1A_{2u} \leftarrow A_{1g}$, with a very low transition moment. In this case the C_0 vibronic origin line is excited by a molecular transition with a $\bar{\nu}$ of 275 cm^{-1} in the $^1A_{2u}$ state and 295 cm^{-1} in the $^1A_{1g}$ ground state.

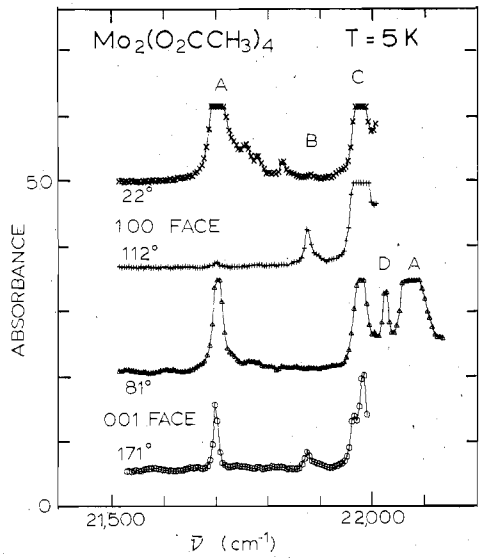

Figure 7. Spectra of thick crystals of $Mo_2(O_2CCH_3)_4$ close to B_{max} and B_{min} for the 100 face and the 001 face of thick crystals. The 100 face was for a crystal 60 μm thick so absorbances can be converted to molar absorptivities by multiplying by 32. The 001 face was for a crystal 37 μm thick so absorbances can be converted to molar absorptivities by multiplying by 53.

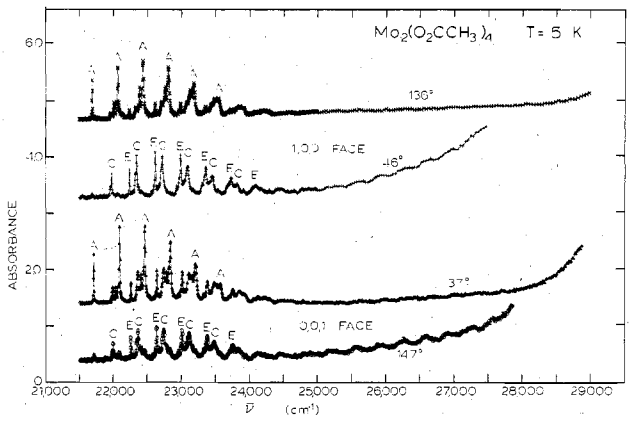

Figure 8. Crystal spectra over the measurable range for the 100 and 001 faces of $Mo_2(O_2CCH_3)_4$. The crystals were 3.8 μm thick for the 100 face and 4.1 μm thick for the 001 face. Polarizations were selected which approximately gave maximum and minimum absorbances at 26 600 cm^{-1}.

In Figure 6 it can be seen that the 21 300- and 21 405-cm^{-1} peaks have comparable intensities at 85 K. The 21 300-cm^{-1} peak grows faster as the temperature is increased, consistent with a higher Boltzmann factor based on the higher 406-cm^{-1} vibration in comparison to 295 cm^{-1}.

Vibrational Features. A number of vibrations in the excited state may now be assigned from the spectra in addition to the A_{1g} metal–metal stretch of 370 cm^{-1}. The 275-cm^{-1} and the 545-cm^{-1} vibrations which excite the *C* and *E* progressions are presumably E_g vibrations. Apparently, only two of the five E_g degenerate pairs of vibrations of the Mo–O–C framework interact effectively with the electronic states to give intense vibronic lines in the spectra. There is a weak 299-cm^{-1} line seen in the Raman spectra which would correspond to the vibration exciting the *C* progression. This would presumably be primarily an Mo–O stretch although Bratton et al.[14] did not place an E_g vibration in this vicinity from force field calculations of the Mo_2O_8 skeleton. There also is a very weak Raman line reported at 567 cm^{-1} which could be the ground state value for the vibration exciting the E_0 line 545 cm^{-1} above A_0. This vibration is presumably a ring deformation which will involve motion of the molybdenum atoms.

The D_0 peak intensity follows that of A_0 as a function of polarization angle. It then could be due to the addition of an A_{1g} vibration of 320 cm^{-1} on to the 0–0 energy. This should also give a Franck–Condon (F-C) progression but the F-C factors are so small that only the first peak above 0–0 is discernible. It was also noted that the F_0 and G_0 peaks fall 315 and 320 cm^{-1} above the C_0 and E_0 peaks, respectively, and could therefore represent the addition of this same A_{1g} energy onto those vibronic origins. This could be associated with the 322-cm^{-1} weak line in the Raman spectrum.

Although the A_0 and E_0 peaks are very narrow and isolated from other features in Figures 2 and 3, both the A_1 and E_1 peaks have weak absorption at about 20 cm^{-1} lower energy, i.e., about 350 cm^{-1} above the origin lines. However, there is no Raman line for a $\bar{\nu}^0$ which might be associated with the $\bar{\nu}'$. Since there are strong IR vibrations at 338 and 350 cm^{-1}, it seems these weak features may be due to vibronic excitations, forbidden in D_{4h}, which become allowed in the lower crystal site symmetry. They would be required to have gerade symmetry, however.

It was apparent from the spectra in Figures 1 and 2 that there was an absorption feature, labeled *B*, at 21 875 cm^{-1}, 175 cm^{-1} above A_0. Therefore spectra for 001 and 100 faces of thick crystals were recorded as functions of polarization angles. Uncertainties in the polarizations of B_{max} were about 5° for each face. Spectra close to B_{max} and B_{min} are shown in Figure 7. The B_0 peak was polarized approximately but not exactly opposite to the A_0 peak; i.e., B_{max} was close to A_{min}, etc. However, the polarization ratio was large enough in the two faces that B_0 cannot be assigned to a degenerate pair of transitions. The orientations of the four possible transition moment vectors were found to be 47, 56, 71, and 76° away from *z*. It was not possible to discriminate between any of these vectors by the intensities in the two faces. Calculated ratios for $B_{max}(100)/L(100):B_{max}(001)/L(001)$ ranged from 0.96 to 1.24 for the four indicated possible transition moment vectors, and the observed value was 1.29. The directions of the four vectors, however, range from 72 to 78° away from the **A** transition moment vector. It seems that the direction of the weaker **B** transition moment deviates a greater amount from the molecular axis than does **A** for the stronger transition. Such deviation may therefore be intensity dependent, since the crystal perturbations are relatively more important for weak transitions.

Figure 7 shows the interesting feature that for the 100 face the polarization ratio for A_0 is so great that A_{min} is comparable to B_{min}, whereas for the 001 face, A_{min} is considerably greater than B_{max}. The waves in the recording of zero absorbance to the left of A_0 for the 001 face in Figure 7 are the consequence of interference from multiply reflected beams between the unusually high optical quality faces of this crystal.

The 175-cm^{-1} vibration which would be required to excite the B_0 line is in the expected region of Mo–Mo–O bending vibrations. Apparently, such vibrations are not as effective as a Mo–O stretch in the vibronic excitation process. It is a bit worrisome, but apparently only a coincidence, that the B_0 peak lies exactly 370 cm^{-1}, or the value of $\bar{\nu}_1'$, below the E_0 peak.

The crystal for the 100 face in Figure 7 was sufficiently thick that weak absorption features at 25, 60, and 80 cm^{-1} above A_0, which follow *A* polarization, are clearly evident. These features likely represent phonon bands on the A_0 line. The weak absorption peak at 130 cm^{-1} above A_0 may or may not be a phonon feature as well.

Franck–Condon Parameters. The intensities of successive lines in the *A*, *C*, *E* progressions offer additional supportive evidence that this band is a $^1A_{2u} \leftarrow {}^1A_{1g}$ transition. The crystal spectra over the entire measurable range are presented in

Figure 8 for the 100 and the 001 face. The polarization angles were chosen to give maximum and minimum absorptions at 26 600 cm^{-1}; however, they are not far from the A_{max} and A_{min} polarizations. Hence for one polarization of each face, the A peaks are the major feature, and for the other polarization the E and C peaks are dominant. In the lower spectrum for each face the intensity of the E and C components decrease in height toward a minimum in the absorption, which occurs in the region 24 000–25 000 cm^{-1}. Beyond 25 000 cm^{-1}, a series of seven to eight broad peaks can be seen in a region of increasing intensity. The average separation of these peaks amounts to 350 cm^{-1}. Absorption is rather low throughout this region in the upper spectrum for each face until the tail of an intense absorption band beyond 29 000 cm^{-1} becomes evident. The absorption at energies above 25 000 cm^{-1} must be due to another electronic transition. Since the origin of the transition is not apparent, it will be designated as the 26 500-cm^{-1} band, since the vibrational components appear to be a maximum at about this energy.

When the relative heights of the successive A peaks are examined in Figure 8, it can be seen that they follow a discernibly different pattern from the E or C peaks. Thus the third A peak, designated A_2 in Table II, is the highest, and A_3 is approximately equal to A_1 and greater than A_0. For the E progression the second peak, E_1, is the highest, whereas E_2 is distinctly shorter, and E_3 is comparable to E_0. The C progression generally follows the E pattern. Since each progression is based on the same totally symmetric vibration, the same set of Franck–Condon parameters would normally be expected. However, in case the transition moment for an electric-dipole-allowed transition becomes sufficiently small, a totally symmetric vibration can be significantly involved in the vibronic coupling. The theory for treatment of Herzberg–Teller coupling by a totally symmetric vibration was presented by Craig and Small.[15] They noted that the moment, $\mathbf{M}_{gv^0,fv'}$, can be written as

$$\mathbf{M}_{gv^0,fv'} = \langle \chi_{v^0}(...Q_i...)|M_{g,f}(...Q_i...)|\chi_{v'}(...Q_i...)\rangle \quad (7)$$

The harmonic approximation to this quantity for a transition from the lowest vibrational level of the ground state will be

$$\mathbf{M}_{g0,fv'} = \mathbf{M}_{g,f}(Q_0)\langle \chi_{g0}\|\chi_{fv'}\rangle \equiv \mathbf{M}_0\langle g0\|fv'\rangle \quad (8)$$

where Q_0 is the equilibrium position for the ground state and $\langle g0\|fv'\rangle$ is the vibrational wave function overlap factor, and its square is the normal Franck–Condon factor that gives the sequence of intensities for the lines.

The molecular vibrations cause a breakdown of the harmonic approximation, and if only one normal vibration, Q_i, influences the transition moment, the deviation from the harmonic approximation is given by

$$\mathbf{M}_{fg}(Q) = \mathbf{M}_0 + \mathbf{m}_iQ_i \quad (9)$$

With this value substituted in eq 7 and with the general vibrational wave functions expressed as products of harmonic oscillator wave functions for normal coordinates, the squares of the transition moments, proportional to the line intensities, divided by $\bar{\nu}$, become

$$\mathbf{M}^2_{g0,fv_i'} = [\mathbf{M}_0^2\langle g0\|fv_i'\rangle^2 + 2\mathbf{M}_0\mathbf{m}_i\langle g0\|fv_i'\rangle \times \langle g0|Q_i|fv_i'\rangle + \mathbf{m}_i^2\langle g0|Q_i|fv_i'\rangle^2] \prod_{j\neq i}\langle g0\|fv_j'\rangle^2 \quad (10)$$

For the usual vibronically excited transition, the first two terms vanish because M_0 is zero. Q_i must be nontotally symmetric and only $v_i' = 1$ will produce a nonzero value for $\langle g0|Q_i|fv_i'\rangle$. The normal Franck–Condon factor is then included in the final product. However, if M_0 is not zero and Q_i is totally symmetric, all three terms contribute to the intensity. The center term may become quite important, and as the signs of $\langle g0\|fv_i'\rangle$ and $\langle g0|Q_i|fv_i'\rangle$ can be either positive or negative, there can be drastic alterations in the normal Franck–Condon progressions. The integrals $\langle g0\|fv_i'\rangle$ have been computed for totally symmetric vibrations, from the formulas presented by Hutchisson that are based on harmonic oscillator wave functions. The values of $\bar{\nu}^0 = 406$ cm^{-1} and $\bar{\nu}' = 370$ cm^{-1} are fixed from the Raman and the electronic spectra. Values were obtained for a series of Δr (Å) for the reduced mass of 48, and the set of integrals, which were considered subjectively to give the best fit with the experimental peak heights in the E progression, are given in Table III. The $\langle g0|Q|fv'\rangle$ integrals were evaluated from Hutchisson's formulas by the method of Yeung[17] for this value of Δr_i and a series of trial values of m_i. A set of calculated intensities in reasonable agreement with the first few terms of the A progression is shown in Table III. All sets were normalized to a value of 1.00 for the highest peak in the progression. The indicated increase, Δr, in the metal–metal equilibrium distance in the excited state from that in the ground state is fairly substantial, i.e., 0.11 Å. The indicated value for $m_i\Delta r/M_0$ was 0.30. So a fairly modest value of m_i can result in the type of difference occurring between the A and the C or E progressions. The calculated bands appear to be somewhat narrower than the observed band. A part of this effect may be due to the fact that the origin peaks were so narrow. Thus their peak height alone does not give an accurate measure of intensity because of the breadth of the higher peaks. Even so, the calculated progressions fall off more rapidly than the experimental peaks. Perhaps this is not too surprising, in view of the simplicity of the model. Hutchisson notes that even a small asymmetry in the vibrational potential energy function can modify the calculations considerably. The value of 0.11 Å for Δr is in substantial agreement with the value of 0.1 Å obtained from the Franck–Condon parameters by Trogler et al.,[9] who utilized a method that assumed equal force constants for the electronic excited and ground states.

Table III. Calculation of Intensities from the Franck–Condon (F-C) and the Herzberg–Teller (H-T) Factors

	intensity E progression		intensity A progression	
transition	obsd peak height	calcd[a] F-C only	obsd peak height	calcd[a,b] F-C and H-T
0–0	0.62	0.30	0.69	0.26
0–1	1.00	1.00	0.98	0.97
0–2	0.93	0.94	1.00	1.00
0–3	0.59	0.38	0.74	0.48
0–4	0.33	0.09	0.43	0.13

[a] $\bar{\nu}_0 = 406$ cm^{-1}, $\bar{\nu}' = 370$ cm^{-1}, $\mu = 48$, $r' - r_0 = 0.11$ Å. [b] $m_i = (2.77\ Å^{-1})M_0$.

Consideration of Other Molybdenum(II) Carboxylate Spectra. The preceding analysis of vibrational intensities at low temperatures and in the hot bands has, we believe, presented strong evidence that the "23 000 cm^{-1}" band for $Mo_2(O_2CCH_3)_4$ is an electric-dipole-allowed transition, $^1A_{2u} \leftarrow {}^1A_{1g}$, with an inordinately low transition moment, so that the Herzberg–Teller vibronic excitations provide some comparable intensities, even at helium temperature. The value of 4.32×10^{-9} cm $M\int \epsilon\, d\bar{\nu}$ for an A_{max} spectrum at 300 K was about 1×10^{-3} which is comparable to the oscillator strength that Trogler et al. gave for a solution spectrum of $Mo_2(O_2CCF_3)_4$. As a Mo–Mo $\delta^* \leftarrow$ Mo–Mo δ transition, it attains intensity by the electron transfer from the d_{xy} orbital of one Mo into the d_{xy} orbital of the other. The d_{xy} orbitals have their greatest extension in a plane normal to the metal–metal axis, and therefore none of the $\delta^* \leftarrow \delta$ transitions are particularly

Table IV. Energies of the Origins of Corresponding Intense Vibrational Progressions in the Crystal Spectra of the Carboxylate Complexes of Molybdenum(II)

complex	A_0, cm^{-1}	$C_0 - A_0$, cm^{-1}	$E_0 - A_0$, cm^{-1}	$A_1 - A_0$, cm^{-1}
$Mo_2(O_2CCH_3)_4$	21 700	275	545	375
$Mo_2(O_2CH)_4$	21 870	400	790	350
$Mo_2(O_2CCF_3)_4$	22 070	255	511	360
$K_4Mo_2(O_2CCH_2NH_3)_4 \cdot 4H_2O$	21 510	280	420	350

intense. It is recognized that for the alkylcarboxylates the lowest unoccupied orbital is the π^* orbital involving carbon and oxygen p orbitals. One symmetry-adapted linear combination of the carboxylate π^* orbitals is a basis for the B_{2g} irreducible representation. It is possible, therefore, that this orbital mixes with the Mo–Mo δ orbital somewhat. In fact, the relatively high transition energy of the first band for the carboxylate complexes might result from this stabilization of the δ orbital, for there is no B_{1u} linear combination for the carboxylate π^* orbitals. Involvement of the carboxylate orbitals results in withdrawal of electron population from the vicinity of the metal–metal bond, where the overlap required for the transition dipole moment occurs. The low intensity for this band may therefore result from such reduction in the transition dipole moment.

Xα–scattered wave calculations, performed for the molybdenum(II) tetraformate molecule by Norman and coworkers,[18,19] have predicted that the lowest spin-allowed transition should be the $\delta^* \leftarrow \delta$. To this extent the present results are in agreement with the calculation. However, the indicated theoretical transition energy was only 14 700 cm^{-1}. This computational technique has also placed the $\delta^* \leftarrow \delta$ energy well below the observed first bands for the $Mo_2Cl_8^{4-}$ and $Re_2Cl_8^{4-}$ ions as well. Cotton et al.[20] pointed out that Xα calculated energies for the $\delta^* \leftarrow \delta$ transition in $Tc_2Cl_8^{3-}$ agreed quite well with the first observed band and suggested that for transitions which involve the promotion of one electron from a filled orbital, the difficulty may reside in the means used to resolve the singlet and triplet state energies.

It is possible that the 26 500-cm^{-1} band observed for $Mo_2(O_2CCH_3)_4$ is then the dipole-forbidden $^1E_g \leftarrow {}^1A_{1g}$ ($\pi^* \leftarrow \delta$) transition. Norman et al. calculated this transition to be 25 600 cm^{-1}. This then would be rather close agreement with experiment. It is the only other spin-allowed transition placed below 37 000 cm^{-1} by the theory. It is possible as well that it could be a spin-forbidden transition corresponding to the intense band seen in solution at about 33 000 cm^{-1}.

The greatest pattern of similarity between the high-resolution spectra of the dimolybdenum alkylcarboxylates is the presence of three strong vibrational progressions in bands in the vicinity of 23 000 cm^{-1} corresponding to the *A*, *C*, and *E* progressions of $Mo_2(O_2CCH_3)_4$. The energies of the *A* origin peaks and distances for the *C* and *E* origins above A_0 are given for four carboxylate complexes in Table IV. The $Mo_2(O_2CCH_3)_4$ has the highest metal–metal stretching frequency ν_1', and the acetate and trifluoroacetate have fairly similar values for the vibrational frequencies leading to the *C* and *E* origins. Although the glycine complex has a similar frequency for the C_0 peak as the acetate, the frequency for the E_0 peak is considerably smaller than that for the acetate complex. The formate has considerably higher vibrational frequencies for the *C* and *E* origins, implying a stiffer ring structure for the formate complex.

Other differences between the carboxylate complex spectra are noted as well. The formate spectra[6] were obtained for the 001 face of an orthorhombic crystal, so there was no complication of the direction for the transmitted plane light waves changing with wavelength. With only one face available, the orientation in space of transition moments for individual lines could not be established. Qualitatively, the polarizations of all peaks were opposite to that expected for exactly *z*-polarized lines. However, a shift of 34° of the transition moment for the *A* peak off the *z* axis in a suitable direction (the magnitude found for the acetate crystals) would invert the polarization ratio.

Crystals of $K_4(Mo_2O_2CCH_2NH_3)_4 \cdot 4H_2O$ provided the first polarized spectra of a carboxylate compound, and they are especially important because crystals of this compound are tetragonal.[20] The metal–metal axis is aligned with the *c* axis, so crystal spectra provide directly the molecular polarizations. Unfortunately, vibrational details were not as well resolved as with the other compounds, but these three intense progressions are clearly seen. The *A* progression whose origin is listed in Table IV is clearly *z* polarized, and the *C* and *E* progressions are both *x*,*y*. However, for this crystal there is a weak, *c*-polarized progression, ca. 10% of the intensity of *A*, with an origin 940 cm^{-1} below the *A* origin. At that time, it was proposed that the transition was forbidden in D_{4h} but dipole allowed in the site symmetry S_4. The *A* progression was then thought to be vibronically excited by a 940-cm^{-1} vibration. In view of the present results this seems no longer tenable. Rather, we now believe that the A_0 peak is the origin for a majority component, and the lower energy progression may be the consequence of a minority or defect component. In this crystal the $-NH_3$ groups of the glycine hydrogen bond to neighboring sulfate oxygens. It is suggested that possibly the defects arise from transfer of a small fraction of such protons to the sulfate across the hydrogen bond. It is recognized that spectra and polarizations for defect components in a host crystal may be modified somewhat.[22]

A study of the polarized spectra of tetrakis[μ-(trifluoroacetato)]-dimolybdenum(II) crystals in our laboratory is not yet complete. As indicated in Table IV, these spectra do include three strong progressions. The electronic band does lie at the highest energy for any of the carboxylato complexes. The spectra exhibit an even richer detail of weak vibrational lines than those for the acetate. There are three very weak lines 50, 95, and 120 cm^{-1} below the intense *A* origin line. Trogler et al.[9] reported the last two of these from their spectrum of powder but did not resolve the first. However, we have found no evidence of an absorption in our thickest crystals of their feature at 21 860 cm^{-1}, which they assigned as the 0–0 line. Because of the now strong evidence that the band in the acetate is for a transition to a $^1A_{2u}$ state, we are proposing that the three weak peaks in the trifluoroacetate crystals are the consequence of a second much weaker transition in this region and that A_0 can still be considered the origin of an $^1A_{2u}$ band. Perhaps this weak transition is apparent with the trifluoroacetate complex because the $^1A_{2u}$ state has the highest energy of the group which has been studied. All of the weak features in the trifluoroacetate complex lie at higher energies than the A_0 peaks of the other carboxylate complexes. It seems likely the weak transition is for a spin-forbidden transition, although the presence of a defect component cannot be excluded.

We believe it is clear from the present study that the interesting class of dimeric complexes of molybdenum(II) and rhenium(III) with bridging carboxylate ligands deserves further investigation. Since so frequently the high molecular symmetry is compromised by low crystal site symmetry, it will be important to search for situations where spectra can be recorded for more than just one face or where higher site symmetries may prevail.

Acknowledgment. We wish to acknowledge very helpful discussions with Professors G. J. Small and E. S. Yeung and the assistance of Professor R. A. Jacobson with the X-ray

diffraction. The work was supported by NSF Grant CHE 76-83665. Spectra were recorded in Ames Laboratory, U.S. Department of Energy.

Registry No. $Mo_2(O_2CCH_3)_4$, 14221-06-8.

References and Notes

(1) C. D. Cowman and H. B. Gray, *J. Am. Chem. Soc.*, **95**, 8177 (1973).
(2) A. P. Mortola, J. W. Moskowitz, N. Rosch, C. D. Cowman, and H. B. Gray, *Chem. Phys. Lett.*, **32**, 283 (1975).
(3) F. A. Cotton, B. A. Frenz, B. R. Stults, and T. R. Webb, *J. Am. Chem. Soc.*, **98**, 2768 (1976).
(4) P. E. Fanwick, D. S. Martin, F. A. Cotton, and T. R. Webb, *Inorg. Chem.*, **16**, 2103 (1977).
(5) J. G. Norman and H. J. Kolari, *J. Am. Chem. Soc.*, **97**, 33 (1975).
(6) F. A. Cotton, D. S. Martin, P. E. Fanwick, T. J. Peters, and T. R. Webb, *J. Am. Chem. Soc.*, **98**, 4681 (1976).
(7) P. E. Fanwick, D. S. Martin, Jr., T. R. Webb, G. A. Robbins, and R. A. Newman, *Inorg. Chem.*, **17**, 2723 (1978).
(8) F. A. Cotton, D. S. Martin, T. R. Webb, and T. J. Peters, *Inorg. Chem.*, **15**, 1199 (1976).
(9) W. C. Trogler, E. I. Solomon, Ib Trajberg, C. J. Ballhausen, and H. B. Gray, *Inorg. Chem.*, **16**, 828 (1977).
(10) F. A. Cotton, Z. C. Mester, and T. R. Webb, *Acta Crystallogr., Sect. B*, **30**, 2768 (1974).
(11) D. S. Martin, Jr., *Inorg. Chim. Acta Rev.*, **5**, 107 (1971).
(12) S. Pancharatnam, *Proc. Indian Acad. Sci., Sect. A*, **42**, 86 (1955).
(13) R. F. Stewart and N. Davidson, *J. Chem. Phys.*, **39**, 255 (1963).
(14) W. K. Bratton, F. A. Cotton, and M. DeBeau, *J. Coord. Chem.*, **1**, 121 (1971).
(15) D. P. Craig and G. J. Small, *J. Chem. Phys.*, **50**, 3827 (1969).
(16) E. Hutchisson, *Phys. Rev.*, **39**, 410 (1930); **37**, 45 (1931).
(17) E. S. Yeung, *J. Mol. Spectrosc.*, **45**, 142 (1973).
(18) J. G. Norman, Jr., and H. J. Kolari, *J. Chem. Soc., Chem. Commun.*, 649 (1975).
(19) J. G. Norman, Jr., H. J. Kolari, H. B. Gray, and W. C. Trogler, *Inorg. Chem.*, **16**, 987 (1978).
(20) F. A. Cotton, P. E. Fanwick, L. D. Gage, B. Kalbacher, and D. S. Martin, Jr., *J. Am. Chem. Soc.*, **99**, 5642 (1977).
(21) F. A. Cotton, B. A. Frenz, E. Pedersen, and T. R. Webb, *Inorg. Chem.*, **14**, 391 (1975).
(22) D. P. Craig and S. H. Walmsley, "Excitons in Molecular Crystals", W. A. Benjamin, New York, N.Y., 1968, Chapter 6.

Contribution from the Structural Chemistry Group, Department of Chemistry, Indian Institute of Technology, Madras 600036, India, and Research School of Chemistry, The Australian National University, Canberra ACT 2600, Australia

Electron Paramagnetic Resonance Studies of Two Low-Spin Hexacoordinate Di(tertiary phosphine) Complexes of Nickel(III)

C. N. SETHULAKSHMI,[1a] S. SUBRAMAINAN,[1a] M. A. BENNETT,[1b] and P. T. MANOHARAN*[1a]

Received December 27, 1978

Single-crystal EPR studies on $[Ni(DP)_2X_2]Y$ (DP = *o*-phenylenebis(dimethylphosphine); $X^- = Cl^-, Br^-$; $Y^- = ClO_4^-, PF_6^-$) doped in the corresponding Co(III) lattices are reported. Principal values of *g* and the ligand superhyperfine tensors obtained are $g_{xx} = 2.1123$, $g_{yy} = 2.1157$, $g_{zz} = 2.0089$; for ^{35}Cl, $A_{xx} = 18.3 \pm 1$ G, $A_{yy} = 15.3 \pm 1$ G, $A_{zz} = 17.6 \pm 1$ G and for ^{31}P, $A\sigma = 13 \pm 1$ G, $A\pi = 5 \pm 1$ G, $A_{zz} = 43.6 \pm 1$ G, when $X^- = Cl^-$ and $Y^- = ClO_4^-$. For $X^- = Br^-$ and $Y^- = PF_6^-$, the values are $g_{xx} = 2.0961$, $g_{yy} = 2.1413$, $g_{zz} = 1.9936$; for ^{81}Br, $A_{xx} = 61 \pm 1$ G, $A_{yy} = 26 \pm 1$ G, $A_{zz} = 169 \pm 1$ G and for ^{31}P, *A* has a nearly isotropic value of 20 ± 2 G. Comparison is drawn to the previously studied DAS (*o*-phenylenebis(dimethylarsine)) analogue as well as among themselves.

Introduction

Ni(III) d^7 EPR has been the subject of many investigations reported hitherto in the literature.[2-13] Since the Ni nucleus is indifferent to EPR (natural abundance of even isotopes of Ni being 98.8%), studies on its complexes with group 6 donors have proved to be of only limited information due to lack of hyperfine interaction. But complexes of group 5B donors with almost 100% natural abundance of magnetic isotopes offer a wealth of data that is of considerable importance in the establishment of their electronic structures. The most illustrative case mentionable as a precursor to the present studies is that of the di(tertiary arsine) complex studied by Gray et al.[4] and Manoharan and Rogers.[3] EPR studies on these dihalo complexes reveal a highly delocalized molecular wave function for the unpaired electron as evidenced by the very well resolved superhyperfine structure from all the immediately bonded nuclei of the ligands. Bennett et al.[14] recently reported the synthesis and optical properties of a series of complexes of Ni(III) with DP and we thought it would be interesting to carry out EPR investigations on two of the complexes, namely, $[Ni(DP)_2Cl_2]ClO_4$ and $[Ni(DP)_2Br_2]PF_6$, to understand the nature of bonding from the analysis of superhyperfine coupling to the ligands. Fortunately, diamagnetic host lattices suitable for substitutional incorporation of these were also available.[14]

We describe the EPR of $[Ni(DP)_2Cl_2]ClO_4$ and $[Ni(DP)_2Br_2]PF_6$ in single crystals of the corresponding Co(III) analogues. Preliminary crystal structure data are available only for $[Co(DP)_2Cl_2]ClO_4$,[15] although no morphological details are known. Since there is no a priori requirement to know the molecular dispositions in the lattice for the derivation of principal values of the magnetic tensors,[16] we have gone ahead with single-crystal EPR studies on these systems. From the known geometries of the host lattice environment of the Co(III) ion and from the previous experience of the orientation of magnetic tensors relative to the molecular framework in the case of Ni(DAS),[4] we could obtain all the necessary information to understand the structure and bonding in these complexes. When complete X-ray data and morphological details become available, these results can be easily corroborated with respect to relation between magnetic axes and molecular framework. Powder EPR data have been used judiciously in unequivocally ascertaining the principal values of the magnetic tensors from crystal data. A simple LCAOMO approach has been used in the derivation of bonding parameters.

Experimental Section

$[Ni(DP)_2X_2]Y$ and the Co(III) analogues were prepared according to literature methods.[14] Single crystals for EPR measurements were prepared by slow evaporation of an acetonitrile solution of the Co(III) complex containing 2–3% of the Ni(III) salt. Powder samples were prepared similarly by grinding the microcrystals obtained as above. Solution measurements were made in a 1:1 mixture of acetonitrile and absolute alcohol.

All EPR spectra were measured on a Varian E-4 X-band spectrometer with a 100-kHz modulation. Field calibrations were made by using DPPH. All measurements were made at room temperature unless specified otherwise.

Results and Discussion

1. $Ni^{III}/[Co^{III}(DP)_2Cl_2]ClO_4$. The EPR spectrum of magnetically dilute polycrystalline $[Ni(DP)_2Cl_2]ClO_4$ shown in Figure 1 reveals an orthorhombic **g** tensor with the high-field *g* component containing 17 large intensity lines spaced with a set of smaller intensity lines. (The lowest field lines of this component overlap with the high-field lines of the low-field

0020-1669/79/1318-2520$01.00/0